

Supplemental Materials

Bayesian Evaluation of a Physiologically Based Pharmacokinetic (PBPK) Model for Perfluorooctane Sulfonate (PFOS) to Characterize the Interspecies Uncertainty between Mice, Rats, Monkeys, and Humans: Development and Performance Verification

Wei-Chun Chou, Zhoumeng Lin*

¹ Institute of Computational Comparative Medicine (ICCM), Department of Anatomy and Physiology, College of Veterinary Medicine, Kansas State University, Manhattan, KS 66506, United States

Wei-Chun Chou: weichunc@vet.k-state.edu;

Zhoumeng Lin: zhoumeng@ksu.edu

* **Corresponding author.** Email: zhoumeng@ksu.edu; Phone: +1-785-532-4087; Fax: +1-785-532-4953; Address: 1800 Denison Avenue, P200 Mosier Hall, Institute of Computational Comparative Medicine (ICCM), Department of Anatomy and Physiology, College of Veterinary Medicine, Kansas State University, Manhattan, KS 66506, United States.

Contents

1. Equations and codes for the PBPK model	3
1.1 Uptake and elimination	3
1.2 Transport in the kidney compartment	4
1.3 PBPK model parameters and baseline values	5
2. Preliminary calibration analysis	5
3. Estimation of posterior parameters	6
3.1 Convergence diagnosis	6
3.2 Markov chains trace plots	6
3.3 Posterior parameter sensitivity analysis	6
4. Model evaluation	7
5. Supplementary Tables	10
Table S1a	10
Table S1b	11
Table S2a	12
Table S2b	13
Table S3a	14
Table S3b	15
Table S3c	16
Table S3d	17
6. Supplementary Figures	18
Fig. S1	18
Fig. S2	18
Fig. S3	19
Fig. S4	19
Fig. S5	20
Fig. S6	20
Fig. S7	21
Fig. S8	21
Fig. S9	22
Fig. S10	23
Fig. S11	24
Fig. S12	25
7. Additional files and instructions	26
7.1 Additional files	26
7.2 Instructions on the model code	27
8. Supplementary references	29

1. Equations and codes for the PBPK model

The equations below, along with the parameters in [Table S1a-b](#), specify the PFOS PBPK model. The same equations are used in the PBPK model code provided below.

1.1 Uptake and elimination

The uptake of PFOS administrated via oral gavage was described using a two-compartment gastrointestinal (GI) model. After oral administration of PFOS into the stomach, PFOS enters the small intestine with a rate defined by the gastric emptying time (GE, 1st order rate constant, h⁻¹). Uptake from the stomach was described using a first-order rate constant, k_{0c} , while the first-order rate constant K_{abs} (h⁻¹) was used to describe the uptake of PFOS in the small intestine (h⁻¹). PFOS absorbed from the GI tract is transported to the liver through the portal vein. PFOS administrated intravenously enters directly into systematic circulation. The equations are provided and explained below:

$$R_{ST} = R_{input} - K_{0c} * AST - GE * AST \quad (S1)$$

$$R_{SI} = GE * AST - K_{abs} * ASI - K_{unabs} * ASI \quad (S2)$$

$$R_{absSI} = K_{abs} * ASI \quad (S3)$$

Where R_{input} is the rate of oral administration of PFOS (mg/h); AST is the amount of PFOS in the stomach (mg); K_{unabs} is the rate constant of unabsorbed PFOS to appear in the feces (h⁻¹).

A first-order urinary elimination rate, K_{urine} , was used to describe the excretion of PFOS from the filtrate compartment via the urine. Similarly, a first-order biliary excretion rate, K_{bile} , was used to account for PFOS excreted into the feces via the bile. The amount of unabsorbed dose to appear in the feces was described using first-order constant, K_{unabs} . The **Equation**

S4-S5 describing the process of first-order urinary and fecal excretion processes:

$$R_{urine} = K_{urine} * A_{fil} \quad (\text{S4})$$

$$R_{feces} = K_{bile} * AL + K_{unabs} * ASI \quad (\text{S5})$$

Where R_{urine} and R_{feces} are the urine and fecal elimination rates of PFOS (mg/h), respectively; A_{fil} (mg) is the amount of PFOS in the filtrate compartment; AL (mg) is the amount of PFOS in liver.

1.2 Transport in the kidney compartment

The derivation of Michaelis-Menten parameters based on the *in vitro* to *in vivo* extrapolation was used to describe the active transport of PFOS by basolateral and apical membrane transporters in the proximal tubule cells as described in [Worley and Fisher \(2015\)](#). Due to the lack of data of PFOS, the activity of transport of PFOS was assumed the same with the consequence of PFOA. Measured V_{max} for uptake of PFOA mediated by organic anion transporters Oat1 and Oat3 ($V_{max_baso_invitro}$) was translated to *in vivo* value describing uptake of PFOS (V_{max_baso}) by multiplying with a relative activity factor (RAF_{baso}) and an estimated mass of PTCs (protein). Similarly, the V_{max} for Oatp1a1 was calculated from *in vitro* studies ($V_{max_apical_invitro}$) and then translated to *in vivo* value (V_{max_apical}) by multiplying the relative activity factor (RAF_{api}) and protein. The transporters in the kidney compartment are defined as **Equations S6-S12**:

$$RK_b = RK_b - R_{Cl} - R_{dif} - RA_{baso} \quad (\text{S6})$$

$$RA_{baso} \text{ (mg/h)} = (V_{max_baso} * CK_b) / (K_m_{baso} + CK_b) \quad (\text{S7})$$

$$RA_{apical} \text{ (mg/h)} = (V_{max_apical} * C_{fil}) / (K_m_{apical} + C_{fil}) \quad (\text{S8})$$

$$R_{PTC} = R_{dif} + RA_{apical} + RA_{baso} - RA_{efflux} \quad (\text{S9})$$

$$d(A_{kb})/dt = RK_b \quad (\text{S10})$$

$$d(A_{Cl})/dt = R_{Cl} \quad (\text{S11})$$

$$d(A_{PTC})/dt = R_{PTC} \quad (\text{S12})$$

where the RK_b and R_{Cl} are the rates of change in the amount of PFOS in kidney blood and

filtrate compartments (mg/h), respectively; R_{dif} is the diffusion rate from kidney to PTCs (mg/h); RA_{baso} is the rate of PFOS transport from the plasma to PTCs through basolateral transporters (mg/h); C_{fil} is the concentration of PFOS in the filtrate compartment (mg/L); CK_b is the concentration of PFOS in the kidney plasma; RA_{efflux} is the efflux rate of PFOS from PTCs back into the systemic circulation (mg/h). The transport rates of basolateral (RA_{baso}) and apical transporters (RA_{apical}) were described by Michaelis-Menten equations. The amounts of PFOS in the kidney plasma (**Eq. S10**), filtrate (**Eq. S11**) and PTCs (**Eq. S12**) compartments were obtained by integration of the rate **Equations S1-S9**.

1.3 PBPK model parameters and baseline values

[Table S1a-1b](#) presented below provide all the parameters of the PFOS PBPK model and the values used as the central value (M) for the prior distribution of the population mean (μ) for the Bayesian analysis except for the physiological parameters. Physiological parameters, such as the body weight, tissue volumes, and plasma flow rates obtained from the literature were fixed in the Bayesian analysis. Several chemical-specific parameters ([Table S1b](#)) are refitted with experimental data using Levenberg-Marquardt algorithm. More detailed notes are included in the footnote of [Table S1a-1b](#).

2. Preliminary calibration analysis

Several chemical-specific parameters whose initial values were obtained from the literature for PFOA were needed to be calibrated with experiment data for PFOS. A preliminary sensitivity analysis (SA) for the PBPK model parameters was performed based on the literature values to select sensitive parameters prior to calibration. The purpose of the SA was to compare and select sensitive PBPK parameter to be included in subsequent calibration analysis, starting with the likely sensitive parameters to reduce the computational burden and improve the performance quality. The preliminary sensitivity analysis and subsequent calibration were conducted using R package “FME” ([Brun et al., 2001](#); [Soetaert and Petzoldt, 2010](#)). [Table S2a – 2b](#) presented the sensitive analysis results and the calibrated values for the mouse, rat,

monkey and human models.

3. Estimation of posterior parameters

3.1 Convergence diagnosis

Four Markov chains of 500,000 iterations each, for the mouse, rat, monkey and human models, respectively, were run with the first 250,000 iterations as “burn-in” iterations and the last 50,000 iterations were used as output iterations to check convergences. Corrected Scale Reduction Factors (\hat{R}) were calculated for the four chains to diagnose the convergences of Markov chains based on the method of Brooks and Gelman (Brooks and Gelman, 1998), and Brooks-Gelman multivariate shrink factor (MPSRF) were used to assess whether the independent MCMC chains have converged to a common distribution. The \hat{R} and MPSRF values of population mean (μ) and population variance (Σ^2) in the mouse, rat, monkey and humans are provided in [Table S3a-d](#).

3.2 Markov chains trace plots

The Markov chains trace plots and its probability density function plots are shown in [Figs. S1-S8](#), which provide a visualization of the Markov chains' convergences. Specifically, a trace plot for the four chains plots the observed chain value (y-axis) against the corresponding iteration number (x-axis). The density plot for the four chains plots the observed chain value (x-axis) against density (y-axis).

3.3 Posterior parameter sensitivity analysis

A local sensitivity analysis was performed to determine which posterior parameters were most influential on the AUC of plasma, liver and kidney concentrations of PFOS in the mouse (single oral dose to 1 mg/kg/day), rat (daily dosing to 1 mg/kg/day for 98 days), monkey (daily dosing to 0.75 mg/kg/day for 182 days) and human (daily dosing to 4.5 ng/kg/day for 25 years). Each of posterior parameters was increased by 1%, and the corresponding AUC of PFOS concentrations were estimated using **Equation S13** ([Lin et al., 2011](#); [Mirfazaelian et al., 2006](#)) as shown below:

$$\text{NSC} = (\Delta r/r * p/\Delta p) \times 100\% \quad (\text{S13})$$

where r is the response variable, and Δr is the change of the response variable resulting from 1% increase in the parameter value, p is the original value of the parameter of interest, Δp is 1% of the original value of the posterior parameter. The relative influence of each parameter on the response variables was categorized as: low: $|\text{NSC}| < 20\%$; medium: $20\% \leq |\text{NSC}| < 50\%$; high: $50\% \leq |\text{NSC}|$ (Lin et al., 2013; Yoon et al., 2009).

4. Model evaluation

The *in vivo* toxicokinetic datasets in mice, rats, monkeys and humans was searched and a few studies that were not included in previous PBPK modeling studies were identified (Fabrega et al., 2014; Kim et al., 2016). The selected toxicokinetic studies for the PBPK model calibration, optimization, and evaluation are listed in Table 1. Key *in vivo* studies are described with more details below:

Mouse

Due to limited datasets in the mouse, all datasets were used for the mouse model development (i.e., calibration and optimization). Two datasets from the same study (Chang et al., 2012) were used for the model calibration and optimization. In this study, the CD-1 male and female mice were administered PFOS as a single oral dose of 1 or 20 mg/kg. At designated times (2, 4, 8 hours and 1, 8, 15, 22, 36, 50, 64 and 141 days) post-dosing, four mice/sex were sacrificed and blood, kidney, and liver samples were obtained. Only male data were used in our study. The comparisons of the mouse experimental data and model predictions are shown in Fig. S9.

Rat

Three oral data sets from 3M unpublished studies (extracted from Loccisano et al. (2012)) with single oral doses (2 and 15 mg/kg) and daily oral dosing (1 mg/kg for 28 days), and the single oral dose studies from Kim et al. (2016) (2 mg/kg) and Chang et al. (2012) (4.2 and 15 mg/kg) were used to develop the PFOS PBPK model for the male rat. In addition to the oral

studies, two single IV studies from [Johnson et al. \(1979\)](#) (single IV of 4.2 mg/kg) and [Kim et al. \(2016\)](#) (single IV of 2 mg/kg) were included for the model development. Moreover, the model was validated against a dietary dosing study (0.5, 2, 5, and 20 ppm for 14 weeks) from [Seacat et al. \(2003\)](#). This study provided exposure information including weekly changes in body weights and food intakes of the rat, allowing incorporation into the model for independent evaluation. The comparisons of the rat experimental data and model predictions are shown in [Fig. S10](#). The independent evaluation result is shown in [Fig. 5](#).

Monkey

Two toxicokinetics datasets for PFOS in cynomolgus monkeys via IV and oral dose routes were used to develop the monkey PBPK model and for model evaluation ([Chang et al., 2012](#); [Seacat et al., 2002](#)). The IV dataset is described in details in [Chang et al. \(2012\)](#). In brief, male and female monkeys (n = 3/sex) were administrated a single IV dose of 2 mg/kg PFOS and then monitored for 161 days after dosing. PFOS concentrations were measured in the plasma and urine of the monkey at several time points (2 – 161 days). Another dataset used for model optimization was from a subchronic toxicity study of PFOS from [Seacat et al. \(2002\)](#). In this study, male and female monkeys received daily oral dosing (by capsule) of 0.03, 0.15, 0.75 mg/kg PFOS for 26 weeks. The animals at the 0.15 and 0.75 mg/kg dose groups were allowed to recover for a year. Serum PFOS concentrations were measured throughout the dosing period for all the dose groups, and also during the recovery period for the 0.15 and 0.75 mg/kg dose groups. The liver PFOS concentration was used for model evaluation from the same dataset ([Seacat et al., 2002](#)). The comparisons of the monkey experimental data and model predictions are shown in [Fig. S11](#). The independent evaluation result is shown in [Fig. 5](#).

Human

The human PFOS toxicokinetic datasets were relatively limited. There were no time-course data with unknown exposure information available in humans, thus only one dataset ([Haug et al., 2009](#)) was considered in our model calibration and optimization. From Haug's

study, the PFOS concentrations were measured in 57 pooled archived human serum samples in the period from 1976 to 2007 (Haug et al., 2009) and this dataset was used in the human model calibration and optimization. Due to lack of exposure information in the model calibration, the exposure ranges of 3.0×10^{-3} $\mu\text{g}/\text{kg}/\text{day}$ before 2000 (exposure time from 1976 to 2000) and 1.9×10^{-3} $\mu\text{g}/\text{kg}/\text{day}$ after 2000 (exposure time from 2001 to 2006) have been used in the simulation of general population from another PBPK modeling study (Loccisano et al., 2011), and thus were applied in our model. In terms of independent data, only sparse datasets (i.e. only one or a few time points per exposure scenario) from epidemiology studies (Olsen et al., 2003a; Olsen et al., 2003b; Olsen et al., 2008) and human autopsy (Fabrega et al., 2014) were available. The human serum PFOS concentrations were measured using samples from the general population from Red Cross adult donors in six cities around U.S. (N=600) from 2000-2001 to 2006 (Olsen et al., 2003a; Olsen et al., 2008). Consistent with the assumption of previous PBPK modeling study (Loccisano et al., 2011) and estimated in the study of Olsen (Olsen et al., 2003a; Olsen et al., 2008), the constant exposure doses were assumed to be the range of 0.0045 $\mu\text{g}/\text{kg}/\text{day}$ before 2000 (simulation time from that 3M began to produce PFOS to the year of phasing out PFOS; 1950s to 2000) and 0.0018 $\mu\text{g}/\text{kg}/\text{day}$ after 2000 (simulation time from 2001 to 2006). The liver PFOS concentration data were collected from International Institute for the Advancement of Medicine (Olsen et al., 2003b), and only the male data (n= 16, age range 5-74) were used in the present study. In addition, the PFOS concentrations in target organs from an autopsy were also used to evaluate the model (Fabrega et al., 2014). However, the detailed exposure information was not available in the human autopsy study. In the human autopsy study, the exposure dose was assumed to 0.0018 $\mu\text{g}/\text{kg}/\text{day}$ (Domingo et al., 2012). Based on the previous report (Haug et al., 2010), food is the major exposure source of PFOS (about 88% - 99%). Thus, all datasets were simulated assuming to be oral exposure. The comparisons of the human experimental data and model predictions using the final optimized parameters are shown in Fig. S12. The model evaluation was shown in Fig. 5.

5. Supplementary Tables

Table S1a

Physiological parameters for the PFOS PBPK model in the mouse, rat, monkey and human.

Parameter	Definition	Units	Baseline value				Source
			Mouse	Rat	Monkey	Human	
BW	Body weight	Kg	0.025	0.3	3.5	82.3	1
QCC	Cardiac output	L/h/kg ^{0.75}	16.5	14	18.96	12.5	2
QLC	Fractional blood flow to liver	Unitless	0.161	0.183	0.194	0.250	2
QKC	Fractional blood flow to kidney	Unitless	0.091	0.141	0.123	0.175	2
HTC	Hematocrit	Unitless	0.48	0.46	0.42	0.44	3
VplasC	Fractional volume of plasma	L/kg BW	0.049	0.0312	0.0448	0.0428	4
VLC	Fractional volume of liver	L/kg BW	0.055	0.035	0.026	0.026	2
VKC	Fractional volume of kidney	L/kg BW	0.017	0.0084	0.004	0.004	2
VfilC	Fractional volume of filtrate	L/kg BW	0.0017	0.00084	0.0004	0.0004	5
VPTCC	Fractional volume of proximal tubule cells	L/g kidney	1.35e ⁻⁴	1.35e ⁻⁴	1.35e ⁻⁴	1.35e ⁻⁴	6
Protein	Amount of protein in proximal tubule cells	mg protein/proximal tubule cell	2.0e ⁻⁶	2.0e ⁻⁶	2.0e ⁻⁶	2.0e ⁻⁶	7
GFRC	Glomerular filtration rate constant	L/h/kg kidney	59	62.1	21.85	24.19	8
GEC	Gastric emptying rate constant	/h/kg BW ^{0.25}	0.54	0.54	2.34	3.51	9

¹ Use measured value if available, or collected from [Brown et al. \(1997\)](#) for mice, rats, and monkeys, and from [ICRP \(2002\)](#) from humans

² Baseline values for the mouse, rat and monkey are from [Brown et al. \(1997\)](#), and the values for the human are from [ICRP \(2002\)](#)

³ Baseline values are from [Hejtmancik et al. \(2002\)](#) (mouse), [Davies and Morris \(1993\)](#) (rat), [Choi et al. \(2016\)](#) (monkey), and [ICRP \(2002\)](#) (human)

⁴ The baseline value was obtained from [Brown et al. \(1997\)](#)

⁵ The baseline value was assumed to be 10% of the kidney volume ([Worley et al., 2017](#))

⁶ Calculated based on 60 million PTCs/g kidney tissue ([Hsu et al., 2014](#))

⁷ All baseline values are from [Addis et al. \(1936\)](#)

⁸ Baseline values are from [Qi et al. \(2004\)](#) (mouse), [Corley et al. \(2005\)](#) (rat, human) and [Iwama et al. \(2014\)](#) (monkey)

⁹ The baseline values of the mouse, rat and human were collected from [Yang et al. \(2015\)](#); the value for the monkey was collected from [Fisher et al. \(2011\)](#)

Table S1b

Chemical-specific parameters for the PFOS PBPK model in the mouse, rat, monkey and human.

Parameter	Definition	Units	Baseline value (Calibrated values)*				Source
			Mouse	Rat	Monkey	Human	
Vmax_baso_invitro	Vmax of basolateral transporters measured in <i>in vitro</i> studies	pmol/mg protein/min	393.45	393.45	439.2	439.2 (479)	1
Km_baso	Km of basolateral transporters	mg/L	27.2	27.2	20.1	20.1	1
Vmax_apical_invitro	Vmax of apical transporters measured in <i>in vitro</i> studies	pmol/mg protein/min	9300 (4185)	9300 (1808)	37400 (76972)	37400 (51803)	1
Km_apical	Km of apical transporters	mg/L	52.3	52.3 (278)	77.5 (45.2)	77.5 (64.4)	1
RAFapi	Relative activity factor of apical transporters	unitless	4.07 (2.81)	3.99 (1.90)	7e-4 (1.4e-3)	7e-4 (1.0e-3)	1
RAFbaso	Relative activity factor of basolateral transporters	unitless	3.99	4.07 (4.15)	1	1	1
KeffluxC	Rate of efflux of PFOS from PTCs into blood	/h/kg BW ^{0.25}	2.49 (5.60)	2.49 (2.09)	0.1	0.1 (0.15)	1
KbileC	Biliary elimination rate constant	/h/kg BW ^{0.25}	4e-3 (3.9e-4)	4e-3 (2.6e-3)	1e-4 (7.8e-4)	1e-3 (1.3e-4)	2
KurineC	Urinary elimination rate constant	/h/kg BW ^{0.25}	1.6	1.6	0.062 (0.092)	0.062 (0.096)	2
Free	Free fraction of PFOS in plasma (male)	unitless	0.09 (0.02)	0.09	0.025 (0.016)	0.025 (0.014)	3
PL	Liver: blood partition coefficient	unitless	3.72 (7.65)	3.72 (3.66)	3.72	2.67 (2.03)	3
PK	Kidney: blood partition coefficient	unitless	0.8	0.8	0.8	1,26	3
PRest	Rest of body: blood partition coefficient	unitless	0.20 (0.23)	0.2 (0.26)	0.2 (0.15)	0.2	2
K0C	Uptake rate constant from the stomach to the liver	/h/kg BW ^{0.25}	1	1	1	1	1
KabsC	Absorption rate constant from small intestine to liver	/h/kg BW ^{0.25}	2.12 (2.53)	2.12	2.12	2.12	1
Kdif	Diffusion rate from kidney plasma to PTCs	/h/kg BW ^{0.25}	0.001 (4.6e-5)	0.001 (5.1e-4)	0.001	0.001	1
KunabsC	Rate of unabsorbed dose to appear in feces	/h/kg BW ^{0.25}	7.05e-5	7.05e-5	7.05e-5	7.05e-5	1

* Calibrated values were refitted from the baseline values with experiment data for each species using the Levenberg-Marquardt algorithm.

¹ The baseline values were assumed to be the same as PFOA in rats from [Worley and Fisher \(2015\)](#) and in humans from [Worley et al. \(2017\)](#). The baseline values of mice and monkeys were assumed to be equal to rats and humans, respectively.

² The baseline values were obtained from [Loccisano et al. \(2012\)](#) (mouse and rat) and [Loccisano et al. \(2011\)](#) (monkey and human).

³ The baseline values were obtained from [Loccisano et al. \(2012\)](#) (mouse and rat), [Loccisano et al. \(2011\)](#) (monkey), and [Fabrega et al. \(2014\)](#) (human). The values for the mouse were assumed to be equal to the rat.

Table S2a

Summary of sensitivity values for parameters

Parameter	Parameter sensitivity value			
	Mouse	Rat	Monkey	Human
Vmax baso invitro	-0.12	-0.04	0.1	-2.3*
Km baso	0.30	0.001	0.2	-0.19
Vmax apical invitro	-1.17*	-0.76*	-21.6*	66.4*
Km apical	0.37	0.84*	8.9*	-72.6*
RAFapi	-0.63*	-0.50*	14.9*	-45.1*
RAFbaso	-0.30	0.51*	0.001	0.001
KeffluxC	0.51*	0.17*	-0.1	-2.1*
KbileC	-3.98*	4.53*	2.6*	24.2*
KurineC	-0.19	0.001	-5.7*	18.0*
Free	-0.48*	-0.08	-7.7*	29.5*
PL	0.57*	-1.50*	-0.7	-3.7*
PK	0.06	0.02	0.001	-0.4
PRest	-0.56*	1.13*	5.1*	0.001
K0C	0.00	0.00	0.001	0.001
Kabsc	-0.72*	0.08	-0.2	0.4
Kdif	1.31*	-0.54*	0.001	-0.19
KunabsC	0.001	-0.07	0.001	0.18

*The absolute sensitivity value of parameters higher than 0.5 was selected for subsequent model calibration analysis.

Table S2b

Calibrated parameter values using the Levenberg-Marquardt algorithm.

Parameter	Unit	Initial value	Calibrated Value
<i>Mouse</i>			
Free	Unitless	0.09	0.02
Vmax_apical_invitro	mg/h/kg BW ^{0.75}	9300	4185
RAFapi	Unitless	4.07	2.81
PL	Unitless	3.72	7.65
PRest	Unitless	0.20	0.23
KeffluxC	/h/kg BW ^{0.25}	2.49	5.60
KbileC	/h/kg BW ^{0.25}	0.004	0.00039
KabsC	/h/kg BW ^{0.25}	2.12	2.53
Kdif	/h/kg BW ^{0.25}	0.001	0.000046
<i>Rat</i>			
Vmax_apicalC	mg/h/kg BW ^{0.75}	9300	1808
Km_apical	mg/L	52	278
RAFapi	Unitless	3.99	1.90
RAFbaso	Unitless	4.07	4.15
PL	Unitless	3.7	3.7
PRest	Unitless	0.2	0.26
KeffluxC	/h/kg BW ^{0.25}	2.49	2.09
KbileC	/h/kg BW ^{0.25}	4e-3	2.6e-3
Kdif	/h/kg BW ^{0.25}	0.001	0.00051
<i>Monkey</i>			
Free	Unitless	0.025	0.016
Vmax_apicalC	Unitless	37400	76972
Km_apical	Unitless	77.5	45.2
RAFapi	Unitless	0.0007	0.001
PRest	Unitless	0.20	0.15
KbileC	/h/kg BW ^{0.25}	1e-4	7.8e-4
KurineC	/h/kg BW ^{0.25}	0.062	0.092
<i>Human</i>			
Free	Unitless	0.025	0.014
Vmax_basoC	mg/h/kg BW ^{0.75}	439	479
Vmax_apicalC	mg/h/kg BW ^{0.75}	37400	51803
Km_apical	mg/L	77.5	64.4
RAFapi	Unitless	0.0007	0.001
PL	Unitless	2.67	2.02
KbileC	/h/kg BW ^{0.25}	0.001	0.00013
KurineC	/h/kg BW ^{0.25}	0.063	0.096
KeffluxC	/h/kg BW ^{0.25}	0.10	0.15

Table S3a

Posterior uncertainty distributions for the population mean (μ) and variance (Σ^2) of the mouse PBPK model parameters.

	Population Geometric Mean (μ)		Population Geometric Standard Deviation (Σ^2)	
Parameters	Median (2.5%, 97.5%)	\hat{R}	Median (2.5%, 97.5%)	\hat{R}
lnVmax_baso_invitro	4.56 (1.50, 5.69)	1.00	-0.54 (-1.70, 1.35)	1.00
lnKm_baso	2.35 (-0.55, 3.17)	1.00	-0.52 (-1.70, 1.45)	1.00
lnVmax_api_invitro	7.83 (4.91, 8.81)	1.00	-0.53 (-1.74, 1.37)	1.01
lnKm_api	4.04 (1.01, 4.95)	1.00	-0.48 (-1.69, 1.55)	1.01
lnRAF_api	0.95 (-2.02, 1.91)	1.00	-0.56 (-1.71, 1.35)	1.00
lnRAF_baso	-0.17 (-3.12, 1.01)	1.01	-0.56 (-1.73, 1.19)	1.01
lnKeffluxC	2.89 (-0.12, 4.01)	1.00	-0.51 (-1.71, 1.21)	1.01
lnKbileC	-7.57 (-7.90, -7.29)	1.01	-0.52 (-1.69, 1.39)	1.01
lnKurineC	-0.07 (-2.92, 0.89)	1.00	-0.54 (-1.72, 1.43)	1.00
lnFree	-3.96 (-5.20, -3.34)	1.00	0.51(-0.71, 2.58)	1.00
lnPL	1.17 (0.73, 1.62)	1.00	0.51 (-0.74, 2.36)	1.00
lnPK	-1.55 (-2.13, -0.01)	1.00	0.51 (-0.74, 2.36)	1.00
lnPRest	-1.78 (-2.96, -1.26)	1.01	-0.55 (-0.68, 2.57)	1.00
lnK0C	-0.43 (-3.46, 0.53)	1.00	0.53 (-0.68, 2.64)	1.00
lnKdif	-9.56 (-12.68, -8.59)	1.00	-0.54 (-0.66, 2.42)	1.00
lnKabsC	0.39 (-2.34, 1.28)	1.00	0.52 (-0.71 2.50)	1.00
lnKunabsC	-10.05 (-13.1, -9.04)	1.00	0.51 (-0.82, 0.95)	1.01

Note: Brooks-Gelman Multivariate Shrink Factors: MPSRF = 1.02.

Table S3b

Posterior uncertainty distributions for the population mean (μ) and variance (Σ^2) of the rat PBPK model parameters.

	Population Geometric Mean (μ)		Population Geometric Standard Deviation (Σ^2)	
Parameters	Median (2.5%, 97.5%)	\hat{R}	Median (2.5%, 97.5%)	\hat{R}
lnVmax_baso_invitro	4.24 (1.18, 5.28)	1.00	-0.53 (-1.69, 1.42)	1.00
lnKm_baso	2.46 (-0.62, 3.50)	1.00	-0.47 (-1.67, 1.51)	1.01
lnVmax_api_invitro	7.57(4.66, 8.45)	1.01	-0.54 (-1.69, 1.37)	1.00
lnKm_api	3.59 (1.24, 5.38)	1.00	-0.52 (-1.71, 1.42)	1.00
lnRAF_api	0.55 (-2.25, 1.34)	1.01	-0.52 (-1.72, 1.26)	1.00
lnRAF_baso	0.35 (-2.67, 1.43)	1.02	-0.53 (-1.74, 1.31)	1.00
lnKeffluxC	0.10 (-2.95, 1.11)	1.00	-0.53 (-1.72, 1.27)	1.01
lnKbileC	-6.65 (-7.02, -6.13)	1.00	-0.49 (-1.69, 1.42)	1.00
lnKurineC	-0.58 (-3.02, 1.11)	1.00	-0.45 (-0.71, 2.54)	1.00
lnFree	-1.92 (-3.88, -1.09)	1.00	-0.48 (-0.70, 2.36)	1.00
lnPL	1.89 (1.37, 2.25)	1.01	-0.49 (-0.67, 2.28)	1.00
lnPK	-0.78 (-3.83, 0.28)	1.00	-0.53(-0.68, 2.51)	1.00
lnPRest	-1.49 (-2.17, -1.19)	1.01	0.50 (-0.68, 2.39)	1.01
lnK0C	-0.24 (-3.22, 0.56)	1.01	-0.46 (-0.69, 2.34)	1.00
lnKdif	-6.77 (-9.85, -5.74)	1.00	-0.45 (-0.69, 2.39)	1.01
lnKabsC	0.13 (-1.85, 0.94)	1.00	-0.46 (-0.70, 0.24)	1.00
lnKunabsC	-7.96 (-11.12, -6.94)	1.00	0.45 (-0.71, 2.54)	1.00

Note: Brooks-Gelman Multivariate Shrink Factors: MPSRF = 1.03.

Table S3c

Posterior uncertainty distributions for the population mean (μ) and variance (Σ^2) of the monkey PBPK model parameters.

	Population Geometric Mean (μ)		Population Geometric Standard Deviation (Σ^2)	
Parameters	Median (2.5%, 97.5%)	\hat{R}	Median (2.5%, 97.5%)	\hat{R}
lnVmax_baso_invitro	6.07 (3.45, 6.68)	1.04	-0.51 (-1.73, 1.29)	1.01
lnKm_baso	0.55 (-0.88, 3.39)	1.00	-0.57 (-1.75, 1.34)	1.01
lnVmax_apical_invitro	10.49 (7.86, 11.71)	1.01	-0.51 (-1.70, 1.28)	1.01
lnKm_apical	3.32 (0.22, 4.32)	1.00	-0.49 (-1.69, 1.40)	1.01
lnRAFapi	-7.52 (-10.08, -6.13)	1.00	-0.61 (-1.76, 1.04)	1.01
lnRAFbaso	0.01 (03.22, 0.61)	1.04	-0.47 (-1.69, 1.70)	1.01
lnKeffluxC	-3.59 (-6.10, -1.86)	1.00	-0.58 (-1.76, 1.38)	1.00
lnKbileC	-7.74 (-8.58, -6.89)	1.01	-0.54 (-1.65, 1.42)	1.01
lnKurineC	-2.90 (-5.98, -1.85)	1.00	-0.57 (-1.77, 1.34)	1.00
lnFree	-4.30 (-7.73, -3.52)	1.02	0.48 (-0.66, 2.58)	1.00
lnPL	1.49 (0.56, 1.94)	1.00	0.49 (-0.71, 2.33)	1.01
lnPK	-0.76 (-3.83, -0.28)	1.01	0.54 (-0.71, 2.26)	1.02
lnPRest	-1.49 (-2.17, -1.19)	1.01	0.50 (-0.68, 2.39)	1.01
lnK0C	-0.51 (-3.65, 0.51)	1.01	0.52 (-0.66, 2.62)	1.02
lnKdif	-9.89 (-10.78, -6.55)	1.01	0.48 (-0.70, 2.21)	1.02
lnKabsc	0.29 (-2.83, 1.26)	1.00	0.43 (-0.75, 2.42)	1.00
lnKunabsC	-10.07 (-13.09, -9.04)	1.01	0.54 (-0.71, 2.57)	1.00

Note: Brooks-Gelman Multivariate Shrink Factors: MPSRF = 1.05.

Table S3d

Posterior uncertainty distributions for the population mean (μ) and variance (Σ^2) of the human PBPK model parameters.

	Population Geometric Mean (μ)		Population Geometric Standard Deviation (Σ^2)	
Parameters	Median (2.5%, 97.5%)	\hat{R}	Median (2.5%, 97.5%)	\hat{R}
lnVmax_baso_invitro	5.58 (2.52, 6.67)	1.00	-0.50 (-1.72, 1.51)	1.00
lnKm_baso	9.47 (6.50, 10.42)	1.01	-0.60 (-1.77, 1.33)	1.02
lnVmax_api_invitro	10.16 (7.29, 11.31)	1.00	-0.44 (-1.68, 1.56)	1.00
lnKm_api	10.76 (7.88, 11.60)	1.01	-0.52 (-1.69, 1.24)	1.00
lnRAF_api	-7.59 (-10.41, -6.45)	1.00	-0.56 (-1.76, 1.28)	1.00
lnRAF_baso	-0.47 (-3.51, 0.52)	1.00	-0.61 (-1.75, 1.47)	1.01
lnKeffluxC	-2.22 (-4.36, -1.38)	1.02	-0.56 (-1.76, 1.51)	1.00
lnKbileC	-9.05 (-12.26, -8.31)	1.01	-0.49 (-1.70, 1.59)	1.00
lnKurineC	-2.65 (-5.64, 1.79)	1.02	-0.45 (-1.72, 1.47)	1.00
lnFree	-4.54 (-7.64, -3.71)	1.01	0.53 (-0.68, 2.58)	1.00
lnPL	0.60 (-2.78, 1.31)	1.00	0.54 (-0.67, 2.52)	1.00
lnPK	-0.26 (-3.40, 0.74)	1.01	0.50 (-0.67, 2.37)	1.00
lnPRest	-1.76 (-4.91, -1.10)	1.01	0.49 (-0.68, 2.42)	1.00
lnK0C	-0.47 (-3.51, 0.51)	1.00	0.51 (-0.66, 2.33)	1.00
lnKdif	-7.40 (-10.52, -6.40)	1.01	0.45 (-0.68, 2.17)	1.00
lnKabsC	-0.30 (-2.77, 1.27)	1.00	0.44 (-0.73, 2.54)	1.01
lnKunabsC	-10.05 (-13.04, -9.04)	1.00	0.49 (-0.69, 2.35)	1.01

Note: Brooks-Gelman Multivariate Shrink Factors: MPSRF = 1.07

6. Supplementary Figures

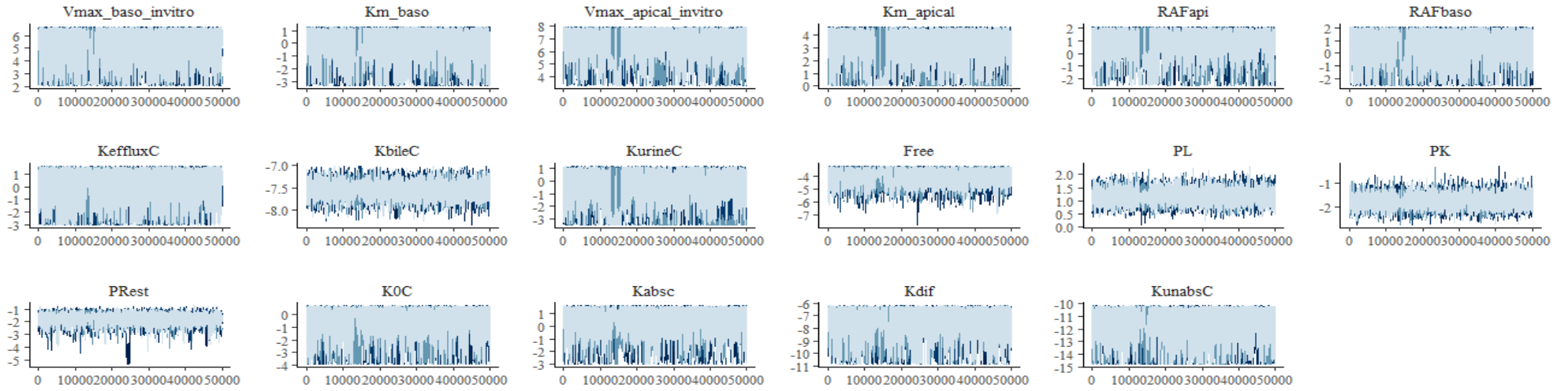


Fig. S1 Traces plot of four Markov chains of the last 50,000 iterations of the MCMC simulation from the mouse model. Gelman and Rubin Shrink Factors: Potential scale reduction factors: $\hat{R} = 1.0 - 1.01$; Brooks-Gelman Multivariate Shrink Factors: MPSRF = 1.02.

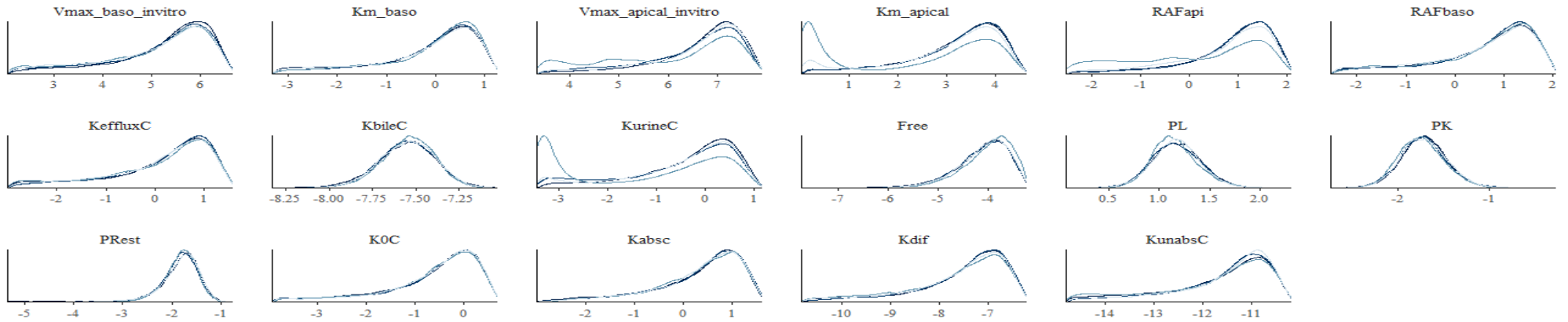


Fig. S2 Probability density function plots of posterior uncertainty distributions for each of the optimized population mean parameters of four Markov Chains from the mouse model

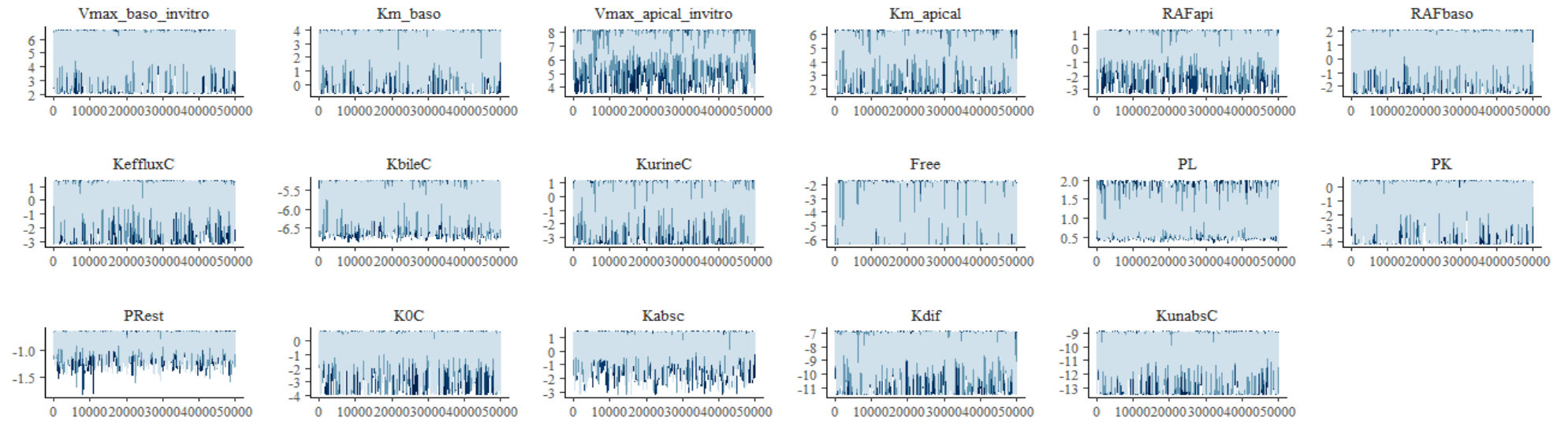


Fig. S3 Traces plot of four Markov chains of the last of 50,000 iterations of the MCMC simulation from the rat model. Gelman and Rubin Shrink Factors: Potential scale reduction factors: $\hat{R} = 1.0 - 1.02$; Brooks-Gelman Multivariate Shrink Factors: MPSRF = 1.05.

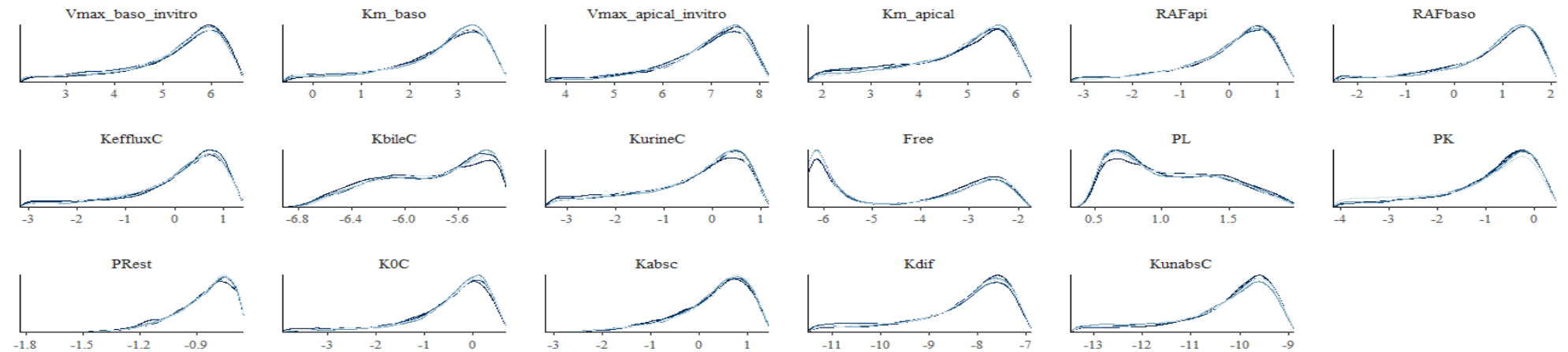


Fig. S4 Probability density function plots of posterior uncertainty distributions for each of the optimized population mean parameters of four Markov Chains from the rat model.

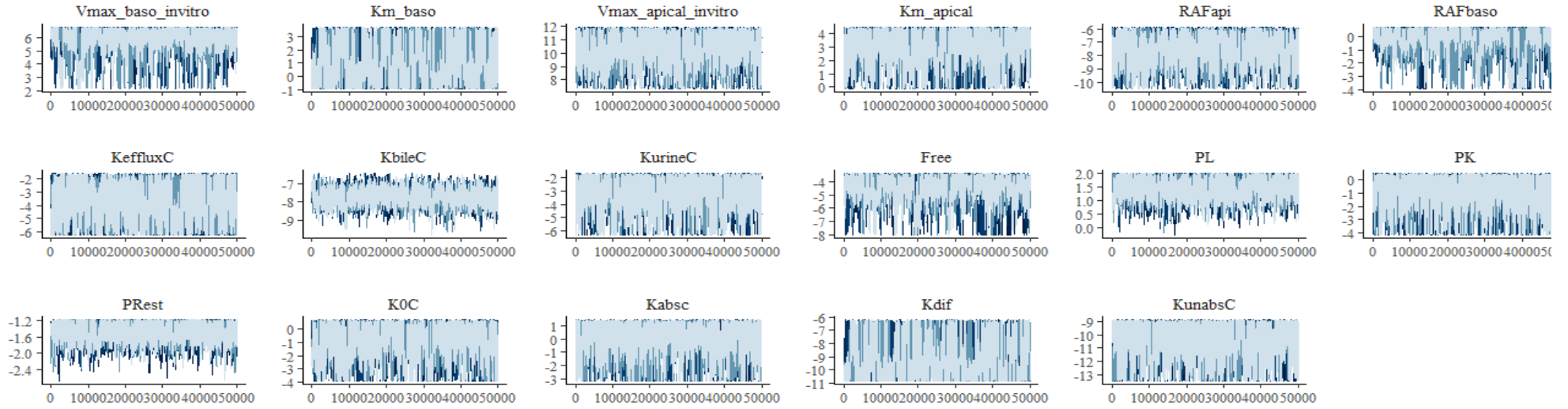


Fig. S5 Traces plot of four Markov chains of the last of 50,000 iterations of the MCMC simulation from the monkey model. Gelman and Rubin Shrink Factors: Potential scale reduction factors: $\hat{R} = 1.0 - 1.04$; Brooks-Gelman Multivariate Shrink Factors: MPSRF = 1.05.

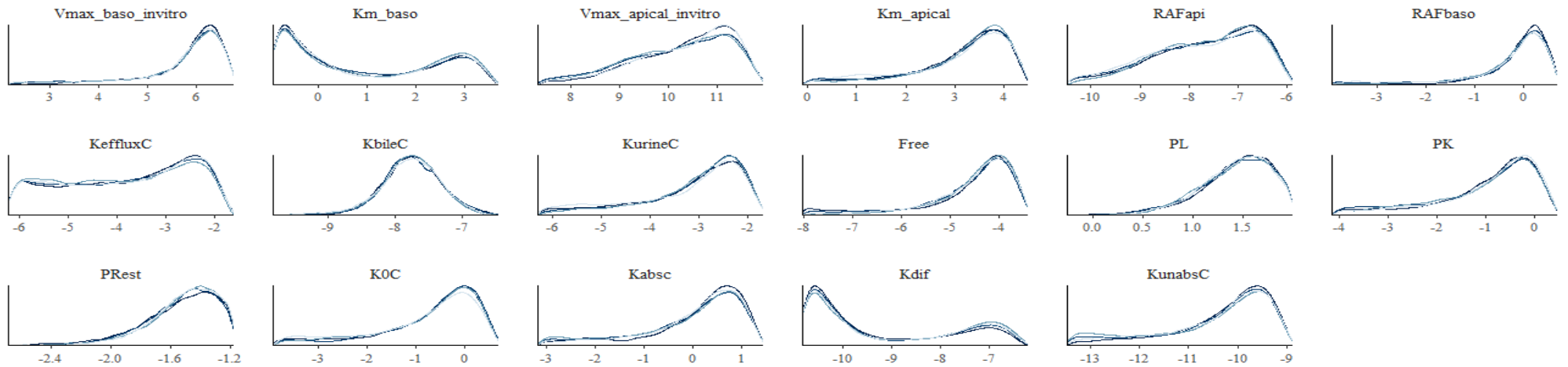


Fig. S6 Probability density function plots of posterior uncertainty distributions for each of the optimized population mean parameters of four Markov Chains from the monkey model.

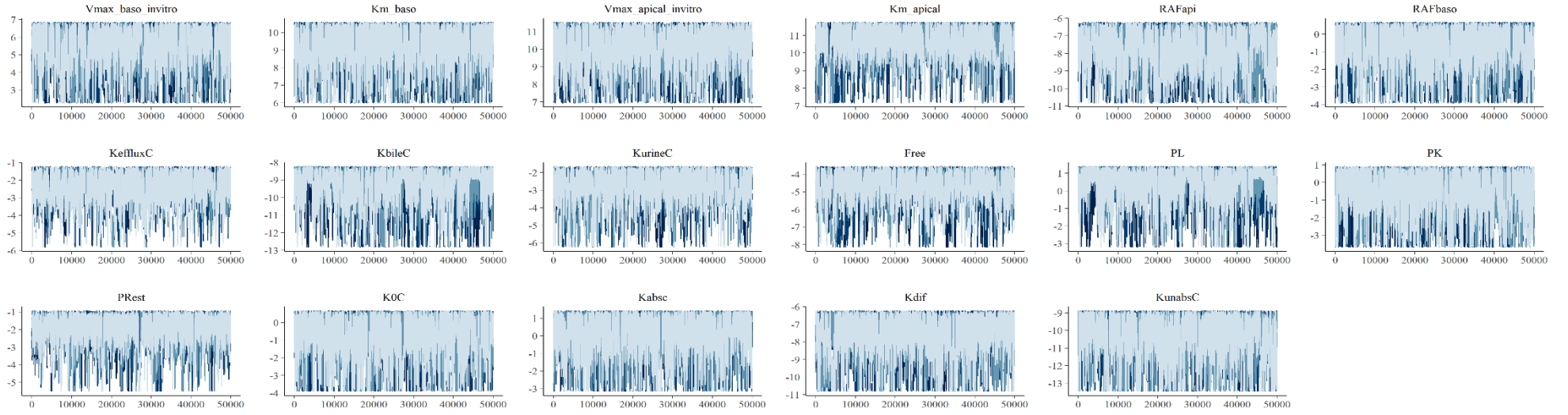


Fig. S7 Traces plot of four Markov chains of the last of 50,000 iterations of the MCMC simulation from the human model. Gelman and Rubin Shrink Factors: Potential scale reduction factors: $\hat{R} = 1.0 - 1.02$; Brooks-Gelman Multivariate Shrink Factors: MPSRF = 1.07.

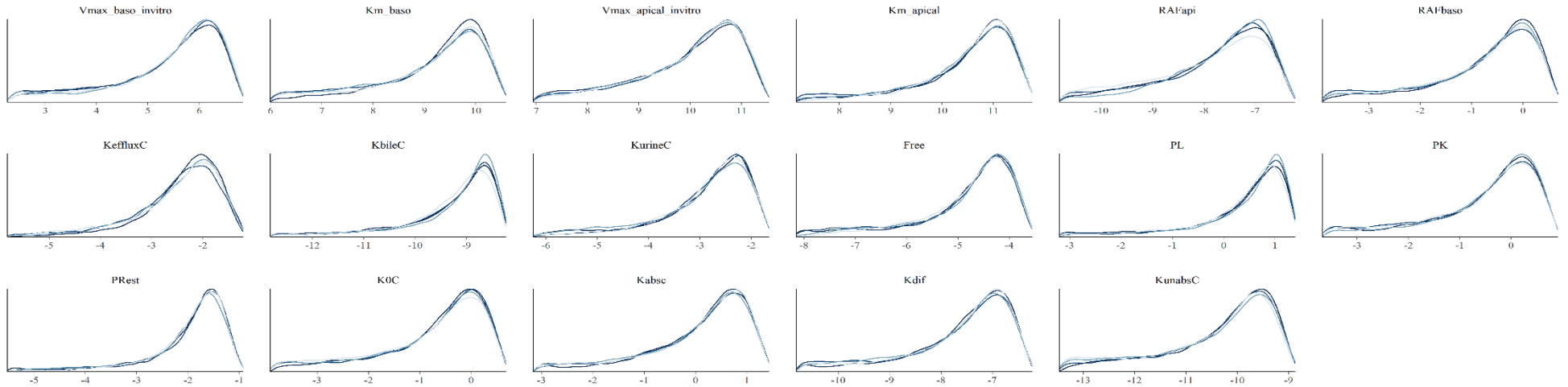


Fig. S8 Probability density function plots of posterior uncertainty distributions for each of the optimized population mean parameters of four Markov Chains from the human model.

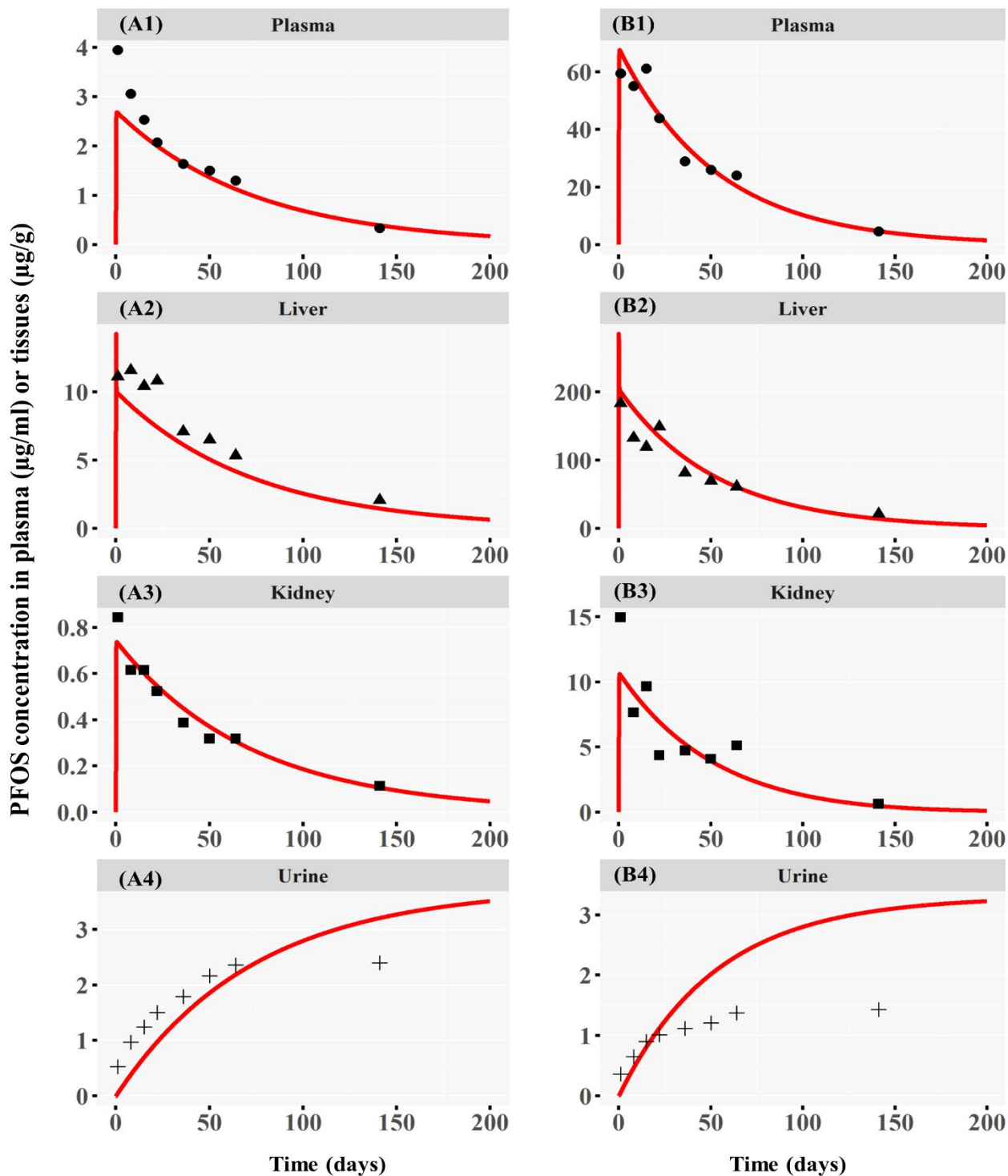


Fig. S9

Comparisons of the PFOS PBPK model predictions for mice with experimental data of single oral dose at (A1-A4) 1 and (B1-B4) 20 mg/kg/day in CD-1 male mice. The experimental data (black dots) are from [Chang et al. \(2012\)](#). The PFOS concentrations were measured in plasma (circle), liver (triangle), kidney (square), urine (cross) and feces (not used in this model).

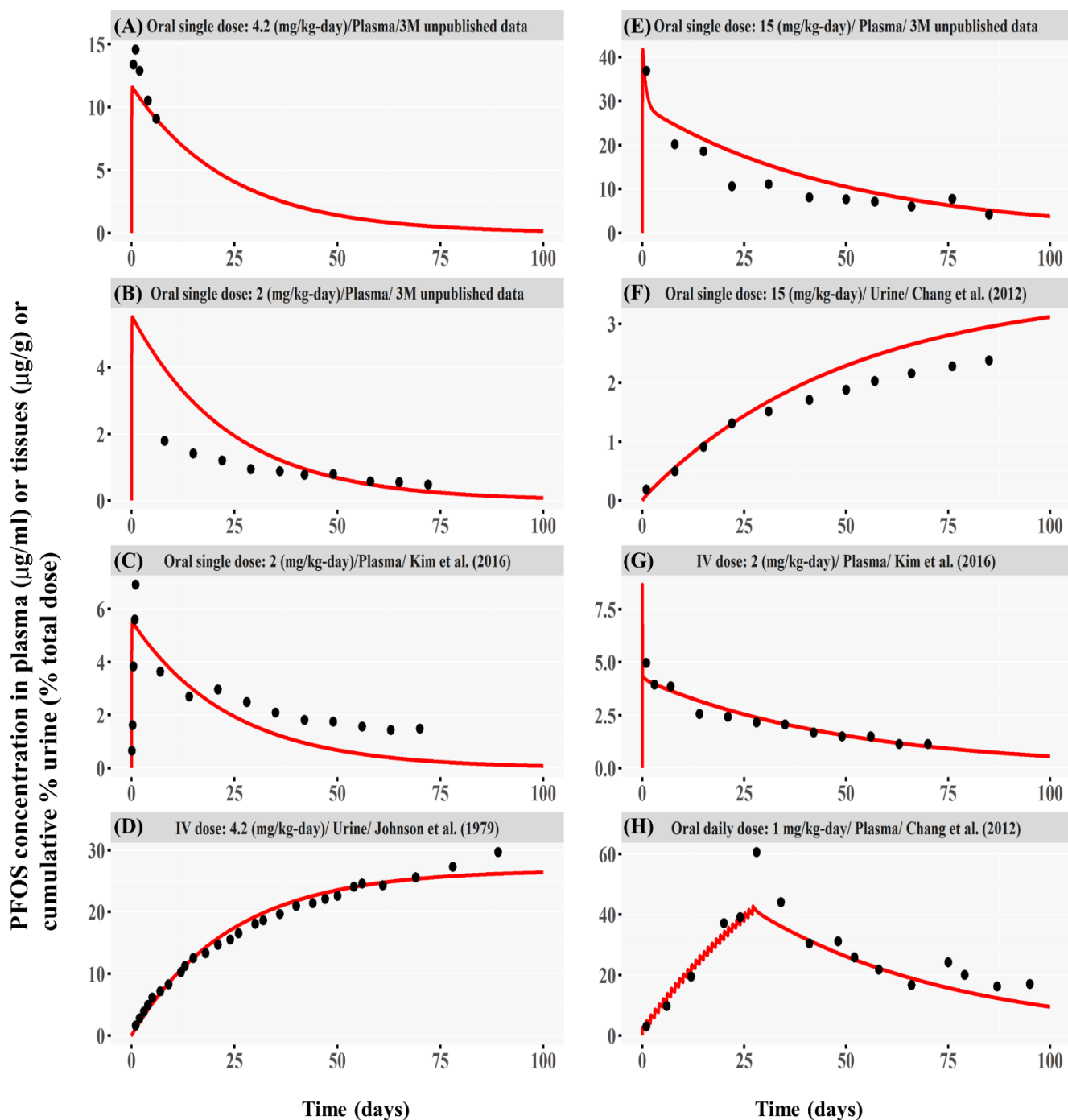


Fig. S10

Comparisons of the PFOS PBPK model predictions for rats with experimental data from single oral (A, B, C, E, F), IV (D, G) and daily oral dosing studies (H) in Sprague Dawley male rats. The experimental data (black dots) are from [3M unpublished data](#), [Johnson et al., 1979](#), [Kim et al., 2016](#) and [Chang et al. 2012](#) (details provided in the Methods section above).

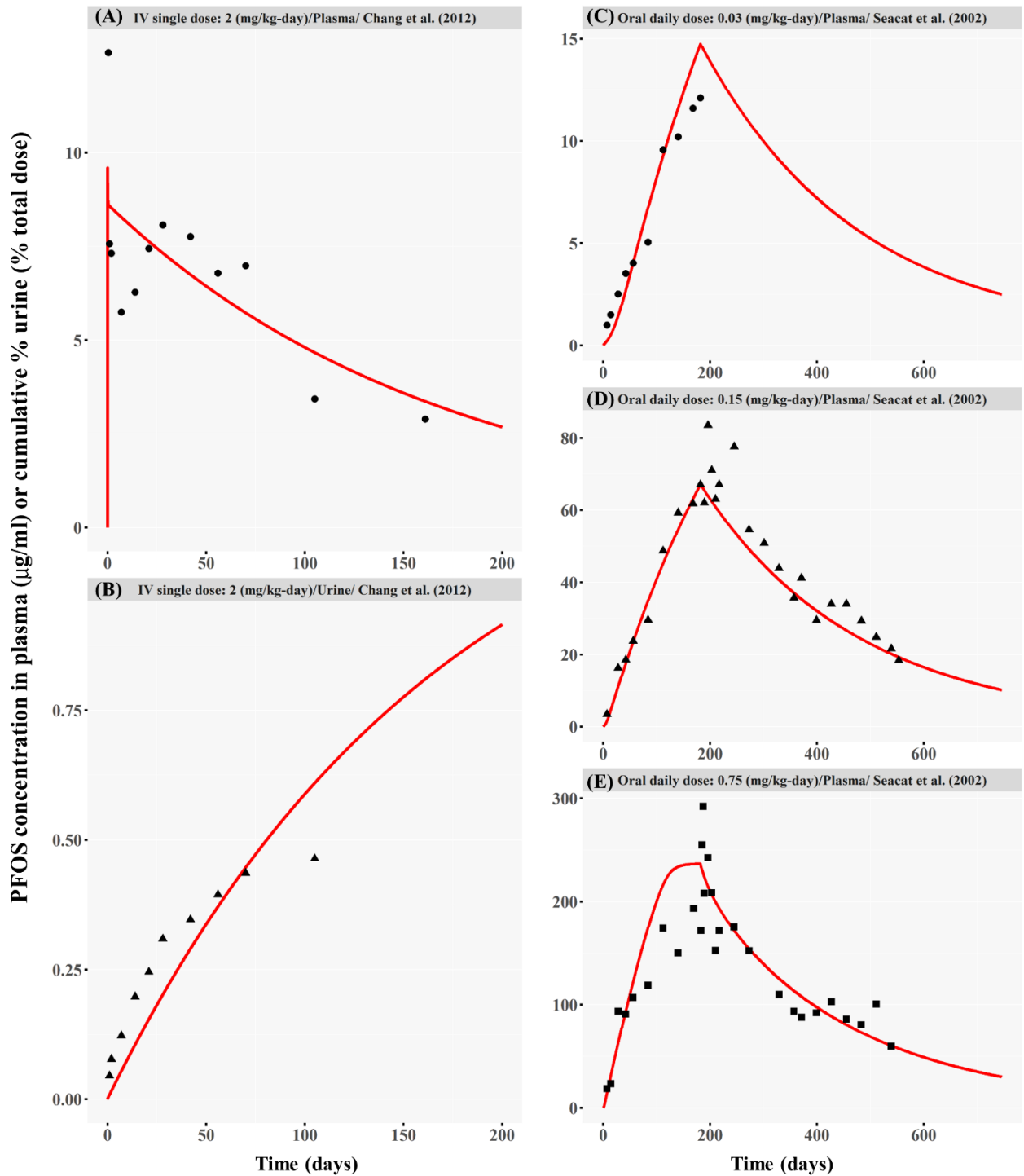


Fig. S11

Comparisons of the PFOS PBPK model predictions for monkeys with experimental data from (A-B) IV and (C-E) daily oral dosing studies in Cynomolgus monkeys. The experimental data (black dots) are from [Chang et al. \(2012\)](#) and [Seacat et al. \(2002\)](#). In the plot A and B, the circle symbols represent plasma data and the triangle symbols represent urine data. In the plot C, D and E, there are three dosing groups treated with 0.03 (circle), 0.15 (triangle), 0.75 (square) mg/kg/day PFOS for 26 weeks. Animals in the dosing groups of 0.15 and 0.75 mg/kg were allowed to recover for one year.

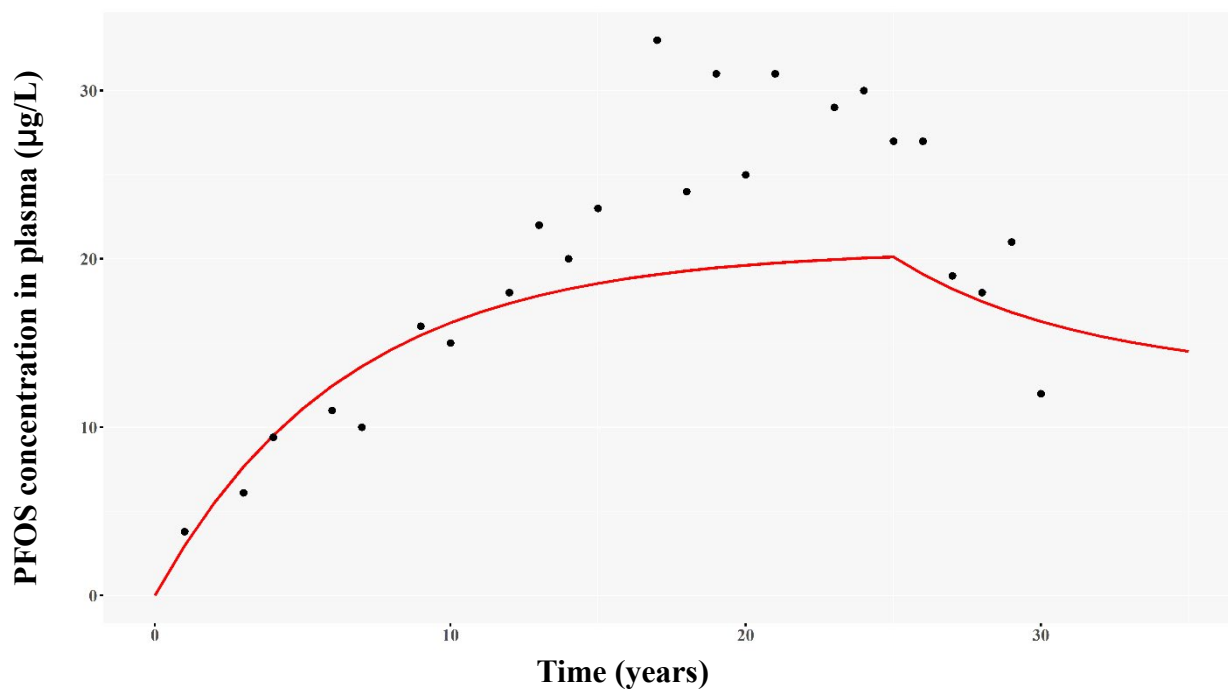


Fig. S12

Comparison of the human PFOS PBPK model predictions of plasma concentrations (solid red line) using the final optimized parameter values with the measured data (black dots) in the archived human serum samples collected from 1976-2007. The experimental dataset is from [Haug et al. \(2009\)](#).

7. Additional files and instructions

7.1 Additional files

The additional files include several separate zip files: **Code.zip**, **Datasets.zip**, and **Results.zip**.

- **Code.zip file:** R codes for model calibration and MCMC optimization in the mouse, rat, monkey and human are included in this zip file.
 - Model fitting & Optimization: The R code for model fitting and MCMC simulation.
 - Mrgsolvecode-Mouse/Rat/Monkey/Human: The R code for mrgsolve-PBPK model code.
- **Datasets.zip file:** All datasets used in model calibration and optimization for the mouse, rat, monkey and human are included in this zip file. Please refer to [Table 1](#) for details.

“Mouse” folder:

- A1: The dataset from [Chang et al. \(2012\)](#): Single oral dose (1 mg/kg); Matrix: plasma.
- A2: The dataset from [Chang et al. \(2012\)](#): Single oral dose (1 mg/kg); Matrix: liver.
- A3: The dataset from [Chang et al. \(2012\)](#): Single oral dose (1 mg/kg); Matrix: kidney.
- A4: The dataset from [Chang et al. \(2012\)](#): Single oral dose (1 mg/kg); Matrix: urine.
- B1: The dataset from [Chang et al. \(2012\)](#): Single oral dose (20 mg/kg); Matrix: plasma.
- B2: The dataset from [Chang et al. \(2012\)](#): Single oral dose (20 mg/kg); Matrix: liver.
- B3: The dataset from [Chang et al. \(2012\)](#): Single oral dose (20 mg/kg); Matrix: kidney.
- B4: The dataset from [Chang et al. \(2012\)](#): Single oral dose (20 mg/kg); Matrix: urine.

“Rat” folder:

- A1: The dataset from [Chang et al. \(2012\)](#). Single oral dose (4.2 mg/kg); Matrix: plasma.
- A2: The dataset from [3M unpublished data](#). Single oral dose (2 mg/kg); Matrix: plasma.
- A3: The dataset from [Kim et al. \(2016\)](#). Single oral dose (2 mg/kg); Matrix: plasma.
- A4: The dataset from [Johnson et al. \(1979\)](#). Single iv dose (4.2 mg/kg); Matrix: urine.
- B1: The dataset from [3M unpublished data](#). Single oral dose (15 mg/kg); Matrix: plasma.
- B2: The dataset from [Chang et al. \(2012\)](#). Single oral dose (15 mg/kg); Matrix: urine.
- B3: The dataset from [Kim et al. \(2016\)](#). Single iv dose (2 mg/kg); Matrix: plasma.
- B4: The dataset from [3M unpublished data](#). Daily oral dose (1 mg/kg) for 4 weeks; Matrix: plasma.

“Monkey” folder:

- A1: The dataset from [Chang et al. \(2012\)](#). Single iv dose (2 mg/kg); Matrix: plasma.
- A2: The dataset from [Chang et al. \(2012\)](#). Single iv dose (2 mg/kg); Matrix: urine.
- B1: The dataset from [Seacat et al. \(2002\)](#). Daily oral dose (0.03mg/kg) for 26 weeks; Matrix: plasma.
- B2: The dataset from [Seacat et al. \(2002\)](#). Daily oral dose (0.15 mg/kg) for 26 weeks; Matrix: plasma.

- B3: The dataset from [Seacat et al. \(2002\)](#). Daily oral dose (0.75 mg/kg) for 26 weeks; Matrix: plasma.

“Human” folder:

- A1: The dataset from [Haug et al. \(2009\)](#). Assumed daily oral dose (3.0e-3 µg/kg-day from 1976-2000, 1.9e-3 µg/kg-day from 2000-2006); Matrix: plasma.

- **Results.zip file:** This zip file contains the R codes used to generate all results presented in the manuscript.

“Code for plots” folder:

- Code for Fig. 3: The R code used to generate results in [Fig. 3](#).
- Code for Fig. 4: The R code used to generate results in [Fig. 4](#).
- Code for Fig. 5: The R code used to generate results in [Fig. 5](#).
- Code for Fig. 6: The R code used to generate results in [Fig. 6](#).
- Code for Table 3: The R code used to generate results in [Table 3](#).
- Code for Table 4: The R code used to generate results in [Table 4](#).
- Code for Fig. S1-S8: The R code used to generate results in [Fig. S1 – S8](#).
- Code for Fig. S9-S12: The R code used to generate results in [Fig. S9 – S12](#).

“Workplace” folder:

- .obs.rds: The “.rds” file containing all observed data for the mouse, rat, monkey and human.
- .MCMC.rds: The “.rds” file containing all results of MCMC simulations for all species.
- .comb.rds: The “.rds” file containing the simulation results of four Markov chains.
- theta.Rat.rds: The “.rds” file containing the calibrated values for parameters.
- PBPK.rds: The “.rds” file containing the PBPK-mrgsolve code.

7.2 Instructions on the model code

This instructions can be separated into three parts, including Part I: model development, Part II: model optimization using MCMC; and Part III: reproducing all figures and tables in the manuscript. The instructions below are presented using the Rat model as an example.

- Open the supplementary files: unzip all zip files → open the folder “Code” → select the “Rat” file → open the R files “**mrgsolvecode-Rat**” and “**Model fitting & Optimization-Rat**” using Rstudio.
- Set your working directory: Set your working directory as the folder “**Data for Rat**” under the folder “**Datasets**”.
- Run the mrgsolve code: Run all the code in “**Mrgsolvecode-Rat**” r file to compile the PBPK model.

Part I: Model development using Levenberg-Marquardt algorithm (Lines 1-247 of the “Model fitting & Optimization-Rat” code file):

- Lines 1–14: loading required R packages

- Line 19: building the mrgsolve-based PBPK model (you need to make sure that you have run all codes in “**mrgsolvecode-Rat**” R file)
- Lines 30–43: input the data sets for model calibration (you need to make sure that you have set the working directory as the folder “**Data for Rat**” under the folder “**Datasets**”)
- Lines 45-199: run the code in lines 45-199. The best-fitting parameters will be generated and saved in the “Fit” object. Using the function “**exp(Fit\$par)**” to check the values of the best-fitting parameters.
- Lines 201-205: to check the fitting results
- Lines 208-247: plot the time-course profiles for the calibration data, the plots are saved in plot.A1, plot.A2, plot.A3, and plot.A4.

Part II: Model optimization with MCMC (Code 250-592)

- Lines 258-269: input the optimization datasets
- Lines 275-313: input the parameters
- Lines 319-435: define the maximum likelihood function
- Lines 439-485: define the prior distribution function
- Lines 487-517: parallel computing + MCMC simulation
- Lines 519- 525: convergence diagnosis for four Markov chains (each of the four chains has 500,000 iterations). The point estimate results represent the \hat{R} ratio results.
- Lines 528: save the posterior parameters (population mean and variance)
- Lines 531-537: convergence plots
- Lines 542-545: save the MCMC results as **.rds** files. “**Rat.MCMC.rds**” is the result of the posterior parameter values from 50,000 iterations.
- Lines 548-592: Plot the time-course profiles for the optimization data, the plots are saved in plot.B1, plot.B2, plot.B3, and plot.B4. The \$bestpar shows the combination of best values for all parameters (i.e., this combination of parameter generates the best fitting results). These values are the final optimized parameter values that were used to generate results in [Fig. 5](#).

Part III: Reproducing all figures and tables presented in the manuscript

- Open the folder “**Results**”. The folder includes two files “**Code for plots**” and “**Workplace**”. The folder “**Code for plots**” stores all r codes for generating results presented in the figures and tables in the manuscript. The “**Workplace**” folder stores the MCMC simulation results for all species, which are saved as different “.rds” files. Please refer to the above for detailed explanation of each “.rds” file.
- Set the working directory as the folder “**workplace**” before running each figure or table code file.
- Open one of the r codes under the folder “**Code for plots**” and run it to reproduce the results presented in the figures and tables in the manuscript.

Part IV: Model application in risk assessment (Reproducing the Table 4)

- Set the working directory as the folder “**workplace**” before running each figure or table code file.
- Open the r codes “**Code for Table 4**” under the folder “**Code for plots**”.
- Lines 1-12: Load required packages
- Lines 14-47: Input the datasets, models and parameters
- Lines 53-178: Define the prediction function for simulations of plasma and liver AUC values in monkeys, rats and humans
- Lines 180-202: The probabilistic AUC was estimated in rats, monkeys and humans from every 10th vector of the final 50,000 MCMC runs. Thus, in total, there were 5,000 iterations, resulting 5,000 AUC values for subsequent calculations of the 95% confidence interval. The simulation of this part of the code will take 12-24 hours depending on your computer.
- Lines 211-215: Estimate the serum AUC, and then divide the AUC by the exposure duration to obtain the average serum concentration (ASC) for rats, monkeys and humans
- Lines 217-221: Estimate the liver AUC, and then divide the AUC by the exposure duration to obtain the average liver concentration (ALC) for rats, monkeys and humans
- Lines 226-227: Derivation of serum dosimetry-derived human equivalent dose (HED) based on the ratios of ASC_{animal} and ASC_{human}
- Lines 228-229: Derivation of liver-dosimetry-derived equivalent dose (HED) based on the ratios of ALC_{animal} and ALC_{human}
- Lines 234-251: Estimate the median (95% CI) of ASC or ALC values
- Lines 254-272: Estimate the median (95% CI) of serum and liver HED values

8. Supplementary references

Addis, T., Poo, L.J., Lew, W., 1936. The quantities of protein lost by the various organs and tissues of the body during a fast. *J. Biol. Chem.* 115, 111–116.

<http://www.jbc.org/content/115/1/111.full.pdf>.

Brooks, S.P., Gelman, A., 1998. General methods for monitoring convergence of iterative simulations. *J. Comput. Graph. Stat.* 7, 434-455. <https://doi.org/10.2307/1390675>.

Brown, R.P., Delp, M.D., Lindstedt, S.L., Rhomberg, L.R., Beliles, R.P., 1997. Physiological parameter values for physiologically based pharmacokinetic models. *Toxicol. Ind. Health.* 13, 407-484. <https://doi.org/10.1177/074823379701300401>.

Brun, R., Reichert, P., Kunsch, H.R., 2001. Practical identifiability analysis of large environmental simulation models. *Water Resour Res* 37, 1015-1030. <https://doi.org/10.1029/2000wr900350>.

Chang, S.C., Noker, P.E., Gorman, G.S., Gibson, S.J., Hart, J.A., Ehresman, D.J., Butenhoff, J.L., 2012. Comparative pharmacokinetics of perfluorooctanesulfonate (PFOS) in rats, mice, and

- monkeys. *Reprod. Toxicol.* 33, 428-440. <https://doi.org/10.1016/j.reprotox.2011.07.002>.
- Choi, K., Chang, J., Lee, M.J., Wang, S., In, K., Galano-Tan, W.C., Jun, S., Cho, K., Hwang, Y.H., Kim, S.J., Park, W., 2016. Reference values of hematology, biochemistry, and blood type in cynomolgus monkeys from cambodia origin. *Lab. Anim. Res.* 32, 46-55. <https://doi.org/10.5625/lar.2016.32.1.46>.
- Corley, R.A., Bartels, M.J., Carney, E.W., Weitz, K.K., Soelberg, J.J., Gies, R.A., Thrall, K.D., 2005. Development of a physiologically based pharmacokinetic model for ethylene glycol and its metabolite, glycolic acid, in rats and humans. *Toxicol. Sci.* 85, 476-490. <https://doi.org/10.1093/toxsci/kfi119>.
- Davies, B., Morris, T., 1993. *Physiological-Parameters in Laboratory-Animals and Humans*. *Pharmaceut. Res.* 10, 1093-1095. <https://doi.org/10.1023/A:1018943613122>.
- Domingo, J.L., Ericson-Jogsten, I., Perello, G., Nadal, M., Van Bavel, B., Karrman, A., 2012. Human Exposure to Perfluorinated Compounds in Catalonia, Spain: Contribution of Drinking Water and Fish and Shellfish. *J. Agr. Food Chem.* 60, 4408-4415. <https://doi.org/10.1021/jf300355c>.
- Fabrega, F., Kumar, V., Schuhmacher, M., Domingo, J.L., Nadal, M., 2014. PBPK modeling for PFOS and PFOA: Validation with human experimental data. *Toxicol. Lett.* 230, 244-251. <https://doi.org/10.1016/j.toxlet.2014.01.007>.
- Fisher, J.W., Twaddle, N.C., Vanlandingham, M., Doerge, D.R., 2011. Pharmacokinetic modeling: prediction and evaluation of route dependent dosimetry of bisphenol A in monkeys with extrapolation to humans. *Toxicol. Appl. Pharm.* 257, 122-136. <https://doi.org/10.1016/j.taap.2011.08.026>.
- Haug, L.S., Thomsen, C., Bechert, G., 2009. Time Trends and the Influence of Age and Gender on Serum Concentrations of Perfluorinated Compounds in Archived Human Samples. *Environ. Sci. Technol.* 43, 2131-2136. <https://doi.org/10.1021/es802827u>.
- Haug, L.S., Thomsen, C., Brantsaeter, A.L., Kvale, H.E., Haugen, M., Becher, G., Alexander, J., Meltzer, H.M., Knutsen, H.K., 2010. Diet and particularly seafood are major sources of perfluorinated compounds in humans. *Environ. Int.* 36, 772-778. <https://doi.org/10.1016/j.envint.2010.05.016>.
- Hejtmancik, M.R., Ryan, M.J., Toft, J.D., Persing, R.L., Kurtz, P.J., Chhabra, R.S., 2002. Hematological effects in F344 rats and B6C3F1 mice during the 13-week gavage toxicity study of methylene blue trihydrate. *Toxicol. Sci.* 65, 126-134. <https://doi.org/10.1093/toxsci/65.1.126>.
- Hsu, V., Vieira, M.D.T., Zhao, P., Zhang, L., Zheng, J.H., Nordmark, A., Berglund, E.G., Giacomini, K.M., Huang, S.M., 2014. Towards Quantitation of the Effects of Renal Impairment and Probenecid Inhibition on Kidney Uptake and Efflux Transporters, Using Physiologically Based Pharmacokinetic Modelling and Simulations. *Clin. Pharmacokinet.* 53, 283-293. <https://doi.org/10.1007/s40262-013-0117-y>.
- ICRP, 2002. Basic anatomical and physiological data for use in radiological protection: reference

- values. A report of age- and gender-related differences in the anatomical and physiological characteristics of reference individuals. ICRP Publication 89. Ann. ICRP 32, 5-265.
- Iwama, R., Sato, T., Sakurai, K., Takasuna, K., Ichijo, T., Furuhashi, K., Satoh, H., 2014. Estimation of Glomerular Filtration Rate in Cynomolgus Monkeys (*Macaca fascicularis*). *J. Vet. Med. Sci.* 76, 1423-1426. <https://doi.org/10.1292/jvms.14-0218>.
- Johnson, J.D., Gibson, S.J., Ober, R.E., 1979. Extent and Route of Excretion and Tissue Distribution of Total Carbon-14 in Rats after a Single Intravenous Dose of ¹⁴C-fc-95-14c. Riker Laboratories, Inc., St. Paul, MN, USEPA Docket No. 8(e)HQ-1180-00374.
- Kim, S.J., Heo, S.H., Lee, D.S., Hwang, I.G., Lee, Y.B., Cho, H.Y., 2016. Gender differences in pharmacokinetics and tissue distribution of 3 perfluoroalkyl and polyfluoroalkyl substances in rats. *Food Chem. Toxicol.* 97, 243-255. <https://doi.org/10.1016/j.fct.2016.09.017>.
- Lin, Z.M., Fisher, J.W., Ross, M.K., Filipov, N.M., 2011. A physiologically based pharmacokinetic model for atrazine and its main metabolites in the adult male C57BL/6 mouse. *Toxicol. Appl. Pharm.* 251, 16-31. <https://doi.org/10.1016/j.taap.2010.11.009>.
- Lin, Z.M., Fisher, J.W., Wang, R., Ross, M.K., Filipov, N.M., 2013. Estimation of placental and lactational transfer and tissue distribution of atrazine and its main metabolites in rodent dams, fetuses, and neonates with physiologically based pharmacokinetic modeling. *Toxicol. Appl. Pharm.* 273, 140-158. <https://doi.org/10.1016/j.taap.2013.08.010>.
- Loccisano, A.E., Campbell, J.L., Andersen, M.E., Clewell, H.J., 2011. Evaluation and prediction of pharmacokinetics of PFOA and PFOS in the monkey and human using a PBPK model. *Regul. Toxicol. Pharm.* 59, 157-175. <https://doi.org/10.1016/j.yrtph.2010.12.004>.
- Loccisano, A.E., Campbell, J.L., Butenhoff, J.L., Andersen, M.E., Clewell, H.J., 2012. Comparison and evaluation of pharmacokinetics of PFOA and PFOS in the adult rat using a physiologically based pharmacokinetic model. *Reprod. Toxicol.* 33, 452-467. <https://doi.org/10.1016/j.reprotox.2011.04.006>.
- Mirfazaelian, A., Kim, K.B., Anand, S.S., Kim, H.J., Tornero-Velez, R., Bruckner, J.V., Fisher, J.W., 2006. Development of a physiologically based pharmacokinetic model for deltamethrin in the adult male Sprague-Dawley rat. *Toxicol. Sci.* 93, 432-442. <https://doi.org/10.1093/toxsci/kfl056>.
- Olsen, G.W., Church, T.R., Miller, J.P., Burris, J.M., Hansen, K.J., Lundberg, J.K., Armitage, J.B., Herron, R.M., Medhdizadehkashi, Z., Nobiletti, J.B., O'Neill, E.M., Mandel, J.H., Zobel, L.R., 2003a. Perfluorooctanesulfonate and other fluorochemicals in the serum of American Red Cross adult blood donors. *Environ. Health Persp.* 111, 1892-1901. <https://doi.org/10.1289/ehp.6316>.
- Olsen, G.W., Hansen, K.J., Stevenson, L.A., Burris, J.M., Mandel, J.H., 2003b. Human donor liver and serum concentrations of perfluorooctanesulfonate and other perfluorochemicals. *Environ. Sci. Technol.* 37, 888-891. <https://doi.org/10.1021/es020955c>.
- Olsen, G.W., Mair, D.C., Church, T.R., Ellefson, M.E., Reagen, W.K., Boyd, T.M., Herron, R.M.,

- Medhdizadehkashi, Z., Nobilett, J.B., Rios, J.A., Butenhoff, J.L., Zobel, L.R., 2008. Decline in perfluorooctanesulfonate and other polyfluoroalkyl chemicals in American Red Cross adult blood donors, 2000-2006. *Environ. Sci. Technol.* 42, 4989-4995. <https://doi.org/10.1021/es800071x>.
- Qi, Z.H., I, W., Mehta, A., Jin, J.P., Zhao, M., Harris, R.C., Fogo, A.B., Breyer, M.D., 2004. Serial determination of glomerular filtration rate in conscious mice using FITC-inulin clearance. *Am. J. Physiol. Renal Physiol.* 286, F590-F596. <https://doi.org/10.1152/ajprenal.00324.2003>.
- Seacat, A.M., Thomford, P.J., Hansen, K.J., Clemen, L.A., Eldridge, S.R., Elcombe, C.R., Butenhoff, J.L., 2003. Sub-chronic dietary toxicity of potassium perfluorooctanesulfonate in rats. *Toxicology* 183, 117-131. [https://doi.org/10.1016/S0300-483x\(02\)00511-5](https://doi.org/10.1016/S0300-483x(02)00511-5).
- Seacat, A.M., Thomford, P.J., Hansen, K.J., Olsen, G.W., Case, M.T., Butenhoff, J.L., 2002. Subchronic toxicity studies on perfluorooctanesulfonate potassium salt in cynomolgus monkeys. *Toxicol. Sci.* 68, 249-264. <https://doi.org/10.1093/toxsci/68.1.249>.
- Soetaert, K., Petzoldt, T., 2010. Inverse Modelling, Sensitivity and Monte Carlo Analysis in R Using Package FME. *J. Stat. Softw.* 33, 1-28. <https://doi.org/10.18637/jss.v033.i03>.
- Worley, R.R., Fisher, J., 2015. Application of physiologically-based pharmacokinetic modeling to explore the role of kidney transporters in renal reabsorption of perfluorooctanoic acid in the rat. *Toxicol. Appl. Pharm.* 289, 428-441. <https://doi.org/10.1016/j.taap.2015.10.017>.
- Worley, R.R., Yang, X.X., Fisher, J., 2017. Physiologically based pharmacokinetic modeling of human exposure to perfluorooctanoic acid suggests historical non drinking-water exposures are important for predicting current serum concentrations. *Toxicol. Appl. Pharm.* 330, 9-21. <https://doi.org/10.1016/j.taap.2017.07.001>.
- Yang, X., Doerge, D.R., Teeguarden, J.G., Fisher, J.W., 2015. Development of a physiologically based pharmacokinetic model for assessment of human exposure to bisphenol A. *Toxicol. Appl. Pharm.* 289, 442-456. <https://doi.org/10.1016/j.taap.2015.10.016>.
- Yoon, M., Nong, A., Clewell, H.J., Taylor, M.D., Dorman, D.C., Andersen, M.E., 2009. Evaluating Placental Transfer and Tissue Concentrations of Manganese in the Pregnant Rat and Fetuses after Inhalation Exposures with a PBPK Model. *Toxicol. Sci.* 112, 44-58. <https://doi.org/10.1093/toxsci/kfp198>.